CrossMark

# Synthesis of novel functional hydrothermal carbon spheres for removal of uranium from aqueous solution

Zhong-jun Lai[3] · Zhi-bin Zhang[1,2,3] · Xiao-hong Cao[1,2,3] · Ying Dai[1,2,3] ·
Rong Hua[1,2,3] · Zhang-gao Le[1,2,3] · Min-biao Luo[1,2,3] · Yun-hai Liu[1,2,3]

**Abstract** A novel chelate sorbent (bis-3,4-dihydroxy-benzy)*p*-phenylen diamine-grafted hydrothermal carbon spheres (HCS-BDBPD) had been successfully synthesized through chemical grafting method. FT-IR and SEM were used to analyze the chemical and microscopy structure of HCS-BDBPD. The batch experiments were carried out to study uranium adsorption properties of HCSs-BDBPD aimed at confirming the optimum condition for removal uranium from waste. The result showed that the sorption process was spontaneous and endothermic in nature and the maximum uranium sorption capacity of 272 mg/g was obtained under the conditions tested, the selectivity of HCSs toward uranium was improved after grafting BDBPD groups on the surface of HCSs.

**Keywords** Uranium · Adsorption · Hydrothermal carbon spheres

✉ Zhi-bin Zhang
zhang_ecut@hotmail.com

✉ Yun-hai Liu
walton_liu@163.com

1   Fundamental Science on Radioactive Geology and Exploration Technology Laboratory, East China Institute of Technology, Nanchang 330013, Jiangxi, China

2   Engineering Research Center of Nuclear Technology Application (East China Institute of Technology), Ministry of Education, Nanchang 330013, Jiangxi, China

3   State Key Laboratory Breeding Base of Nuclear Resources and Environment, East China Institute of Technology, Nanchang 330013, Jiangxi, China

## Introduction

Uranium contaminant often arises as a result of authorized and accidental releases at various stages in the nuclear fuel cycle from uranium ore mining activities to post-reactor operations [1]. The leaked uranium easily occur in aqueous environment such as ground water and surface water [2], posed a threat to human beings due to its heavy metal toxicity and radioactivity. In view of uranium resources recovery and environment protection, diminishing and eliminating uranium in water system is worthy [3].

Separation technologies such as chemical precipitation [4–6], ion-exchange [7], solvent extraction [8] and adsorption have been developed for the treatment of uranium from U-containing waters. Adsorption process owns advantage properties of higher selectivity, faster kinetics and cost advantage [9–12].

Adsorbents play a critical role in uranium adsorption effectivity.

Carbonaceous adsorbents such as mesoporous carbon and hydrothermal carbon have received high attention because of heat and irradiation stability [13, 14]. Mesoporous carbon grafted with various groups possesses unique sorption properties toward uranyl [15–17]. In addition, hydrothermal carbon materials are semi-carbonized material, which can be derived from hydrothermal processing of mono- and polysaccharides with the following features: mild reaction conditions, cheap carbon sources, and completely "green" as it excludes organic solvents, surfactants or ultra-high temperature [18, 19]. Especially, it is praiseworthy that the mild reaction condition in the synthesis procedure results in much more abundant oxygen-containing functional groups (OFGs) on the surface of hydrothermal carbon spheres (HCSs) than that of other carbonaceous materials such as activated carbon materials [20].

🕸 Springer

Surface modification including physical modifications (such as impregnation) and chemical modifications (such as grafting) [21, 22], an efficient route for improving the adsorption capacity and selectivity beyond their existing structural and functional features, has been drawing more attention in recent years. In order to prepare high concentration of OFGs such as carboxyl, oxidation treatment is now a priority candidate [23]. Nevertheless, for chemical oxidation, strong acids or strong oxidants could usually cause collapse and/or corrosion to framework and surface of carbon material [24].

The surface grafting, used in this paper, can avoid the disadvantages, and the grafted functional group (BDBPD) has high affinity to uranium. The HCS-BDBPD was prepared for the first time, and study of uranium adsorption properties of the HCS-BDBPD were conducted by batch experiments.

The aim of the present research was to investigate the sorption properties of HCSs-BDBPD toward U(VI) from aqueous solutions. Various techniques such as Fourier transform infrared spectroscopy (FT-IR) and scanning electron microscopy (SEM) were used to characterize the micro-morphology and structure. The effect of various experimental parameters including pH of the solution, competing ions, contact time, initial concentration, and temperature, as well as adsorption kinetics, isotherm models, and thermodynamics were studied.

# Chemicals and experiment

## Materials

For the preparation of a stock U(VI) solution, 2.9480 g $U_3O_8$ was put in a 100 ml beaker, and 10 ml HCl ($\rho = 1.18$ g/mL) and 2 mL $H_2O_2$(36.5 wt.%) were added. The solution was heated to wet salt shape then 10 mL HCl ($\rho = 1.18$ g/mL) was added. The solution was transferred to a 250 mL flask and diluted to the mark with distilled water to produce a U(VI) stock solution (10 mg/mL). The uranium solutions experiment required were prepared by diluting the stock solution. All other chemicals and reagents such as sodium hydroxide, o-phenylenediamine, ethane diamine, salicylaldehyde, sodium borohydride, dicyclohexylcarbodiimide (DCC), sodium nitrite were purchased from Aladdin Chemistry Co., Ltd., China.

All reagents are of AR degree and used without further purification.

## Preparation of (bis-3,4-dihydroxy benzy)p-phenylen diamine-grafted hydrothermal carbon spheres

The synthesis scheme is illustrated in Fig. 1. (1) 80 mL of glucose solution (20.0 wt.%) was put in a 100 mL Teflon-

lined stainless steel autoclave witch and was then sealed and heated to 453.15 K with a heating rate of 2.5 k/min in an oven. After 24 h, the solution was cooled down to room temperature naturally, was filtered off and washed completely with distilled water, ethanol, and acetone until the filtrate was colorless and nearly neutral, then dried at 323.15 K in vacuum for 8 h. The resulting material was denoted as HCSs. (2) HCSs were calcined in muffle furnace in air at 773.15 K for 5 h to enhance the amount of carboxylic groups on the surface of HCSs, and then the carboxylic hydrothermal carbon spheres were obtained and denoted as HCSs–COOH [25]. (3) Under the condition of stir, 1.0 g of HCSs–COOH was added in 250 mL beaker loaded with 40 mL of ethyl acetate in the ice-bath. After HCSs–COOH was dispersed, 1.0 g of dicyclohexylcarbodiimide (DCC) and 20 mL of ethane diamine was added and then the beaker was shifted out from ice-bath keep stirring for 24 h. The products were filtrated and washed with distilled water and ethanol until the filtrate was nearly neutral, then dried ant 323.15 K in vacuum for 8 h. The obtained material was denoted as HCSs–NH$_2$. (4) The (double-3, 4-2 hydroxy benzyl) para-phenylene diamine (BDBPD) was prepared according to Ref [26]. (5) A
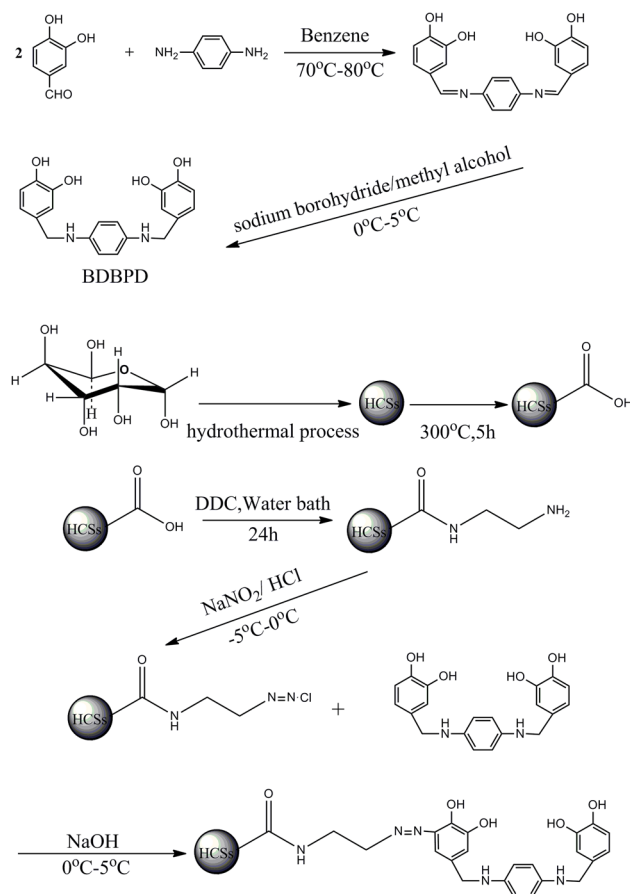


Fig. 1 Preparation of HCSs-BDBPD

certain amount of HCSs–NH$_2$ and sodium nitrite solution (1 mol/L) was added in hydrochloric acid (1 mol/L), and then the mixture reacted under ice-bath condition for 3 h. The product was filtrated and washed with deionized water until the filtrate was nearly neutral. The diazotization hydrothermal carbon spheres were obtained and denoted as HCSs–N=N–Cl. 0.6 g of BDBPD was dissolved in sodium hydroxide solution (10 wt.%) and 0.5 g of HCSs–N=N–Cl was added slowly under ice-bath, then the mixture react for 5 h. The product was filtrated and washed with deionized water until filtrate was nearly neutral, dried in vacuum. The final material was obtained and denoted as (HCSs-BDBPD).

## Characterization

Surface morphology was characterized on a JEOL JSM-5900 scanning electron microscopy. The FT-IR spectra were recorded on Nicolet Nexus 870 Fourier transform infrared spectrometer using the KBr pellet technique (1:50) with the resolution 2 cm$^{-1}$.

## Sorption experiment

The adsorption performance was investigated using the batch wise method. Effects of pH, ionic strength, contact time, initial concentration and temperature on the adsorption were studied. The single factor experiment was operated as following. HCSs or HCSs-BDBPD of 0.01 g was suspended in 100 mL solution of U(VI) of a definite concentration at a certain pH, which was adjusted by 0.1 mol/L HCl and 0.1 mol/L NaOH. The mixture was shaken for desired time, followed by the phased separation using filtration. The obtained supernate was taken and analysed U(VI) concentration using the arsenazo III method with a 721 type spectrophotometer at 650 nm. The adsorbed uranyl ions on per unit mass of the adsorbent were calculated by Eq. 1. [27]

$$q_{\mathrm{e}} = \frac{(C_0 - C_{\mathrm{e}})V}{W} \tag{1}$$

where $q_{\mathrm{e}}$ is the adsorbed U(VI) quality on HCSs–BDBPD (mg/g), $C_0$ and $C_{\mathrm{e}}$ are the initial and equilibrium solution uranium concentrations (mg/L), respectively, $V$ is the volume of the aqueous solution (L) and $W$ is the mass of HCSs-BDBPD (g).

## Results and discussion

### Characterization

The microcosmic morphology of HCSs and HCSs-BDBPD were studied by SEM and shown in Fig. 2. As can be seen

from Fig. 2a (magnified 3000 times), HCSs exhibited regular, uniform and smooth balls. HCSs-BDBPD shown in Fig. 2b (magnified 6000 times) revealed that after functionalization the resultant HCSs-BDBPD still hold physical properties as HCSs.

Figure 3 shows the FT-IR spectra of HCSs, HCSs–COOH, HCSs–NH$_2$, HCSs-BDBPD. The peaks at 3400, 1710, and 1619 cm$^{-1}$ are ascribed to O–H stretching vibration, C=O stretching vibration and C=C stretching vibration [28, 29]. The intensity of the adsorption bands at 1710 and 1619 cm$^{-1}$ were increased obviously in curve a in the Fig. 3 and a new peak can be observed at 1227 cm$^{-1}$ attributed to the carboxylic acid anhydride C–O stretching vibration [30]. These results indicated that the carboxylic groups were grafted on the surface of HCSs successfully. In spectrum of HCSs–NH$_2$ (curve c in the Fig. 3), the peaks at 1674, 1555 and 1300 cm$^{-1}$ belongs to the amide I, II and III stretching vibration respectively [31]. In spectrum of HCSs-BDBPD (curve d in the Fig. 3), the bands at 1463, 1060 and 675 cm$^{-1}$ was corresponded to the aromatic stretching vibration [32, 33]. The band at 1290 and 817 cm$^{-1}$ were assigned to the C–N stretching vibration and the aromatic C–H out-of-plane bending vibration [31, 34]. The results of FT-IR spectra indicate that HCSs-BDBPD was prepared successfully.

### The effect of pH

Due to influencing uranium speciation and surface charge of the adsorbent, the initial pH is one of the most important factors on uranium sorption [35]. The effect of initial pH in the range of 3.0–8.0 on uranium adsorption was conducted and the result was shown in Fig. 4. For HCSs and HCSs-BDBPD, both $q_{\mathrm{e}}$ increased as pH increased from 3.0 to 6.0, decreased as pH beyond 6.0. The optimal pH values were both determined as 6.0 and the corresponding $q_{\mathrm{e}}$ were the maximum of 55.70 and 272.0 mg/g, respectively.

The low adsorption capacity at low pH value could be attribute to the competition of H$^+$ and H$_3$O$^+$ ions with UO$_2^{2+}$ on the adsorptive active sites [25]. As pH increased, the functional groups on the adsorbent surface gradually obtained more adsorption sites for positive uranium species. The adsorption capacity decreased as pH continuously rose from 6.0 to 8.0 because of the hydrolysis of uranyl at higher pH condition [36]. As a consequence, pH of 6.0 is considered as the optimum pH for further experiments.

### The effect of contact time

Contact time is also a critical parameter for uranium adsorption and the effect of contact time on the adsorption properties of HCSs and HCSs-BDBPD are showed in Fig. 5. As can be seen, the amount of adsorbed U(VI) on
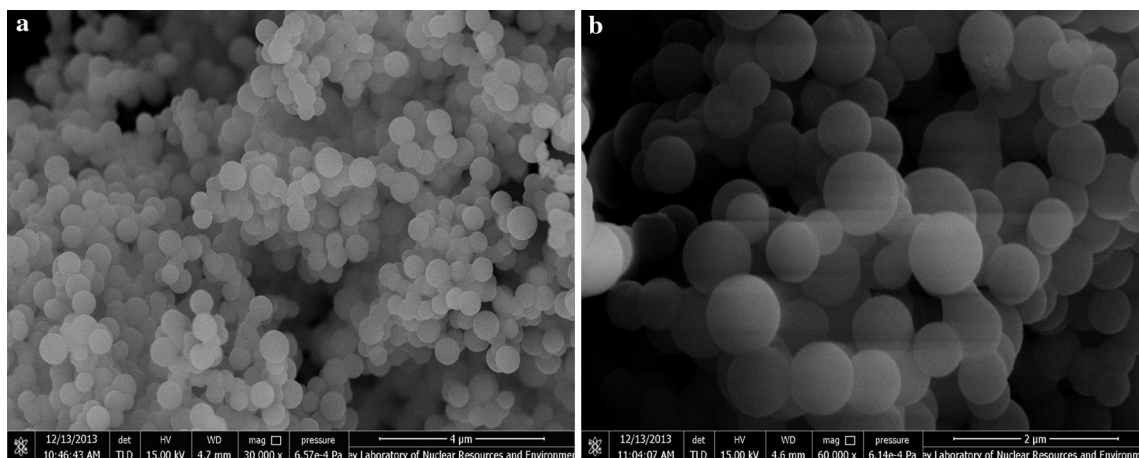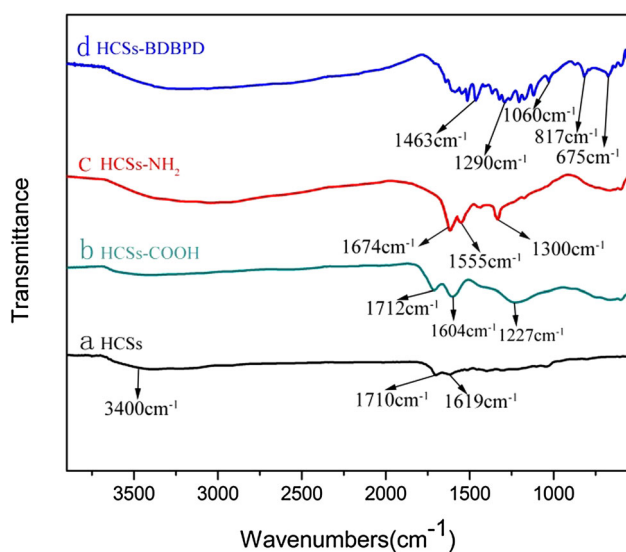
**Fig. 2** SEM images of HCSs (**a**) and HCSs-BDBPD (**b**)



**Fig. 3** FT-IR spectra for HCSs before and after grafting



**Fig. 4** The effect of pH on the adsorption properties of HCSs and HCSs-BDBPD

HCSs and HCSs-BDBPD increased rapidly at the beginning, and finally reached equilibrium after 60 and 90 min, respectively. The faster adsorption rate at the beginning would be due to the larger concentration gradient [14].

Two different kinetic models (pseudo-first-order and pseudo-second-order) were applied to investigate the adsorption rate controlling mechanism of the adsorption process, and the results were showed in Fig. 5. The pseudo-first-order and pseudo-second-order can be written as: [37]

$$\ln(q_e - q_t) = \ln q_e - k_1 t \tag{2}$$

$$\frac{t}{q_t} = \frac{1}{k_2 \cdot q_e^2} + \frac{t}{q_e} \tag{3}$$

where $q_e$ and $q_t$ (mg/g) are U(VI) concentration in solid phase at equilibrium and $t$ (min), respectively. $k_1$ (min$^{-1}$) and $k_2$ (g mg$^{-1}$ min$^{-1}$) are the sorption rate constants of
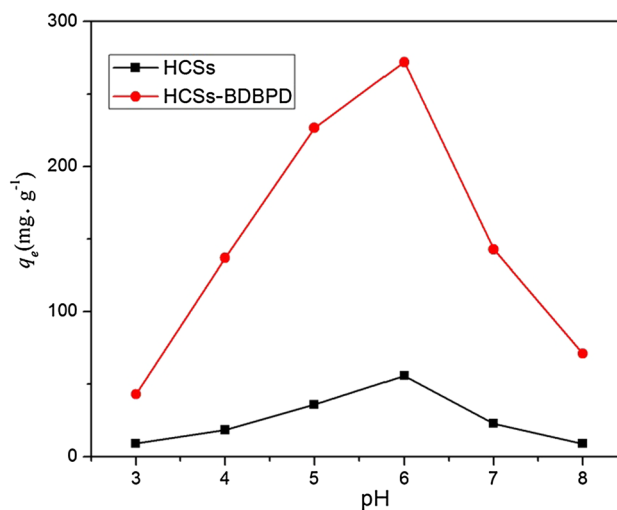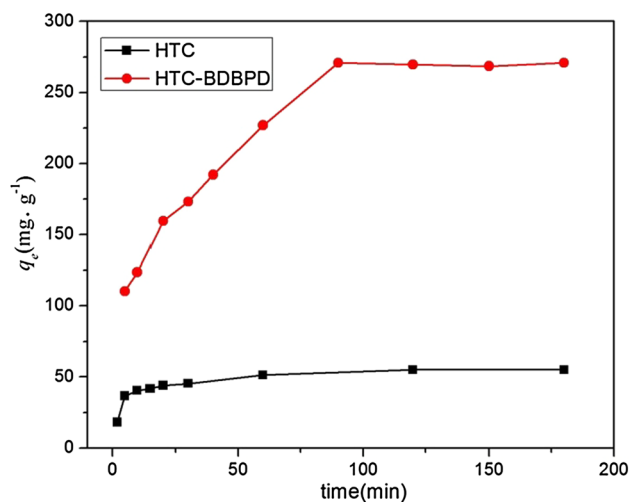


**Fig. 5** Effect of contact time on U (VI) sorption on HCSs and HCSs-BDBPD

pseudo-first-order and pseudo-second-order models, respectively.

The plots of plots of $\ln(q_t - q_e)$ versus $t$ and $t/q_t$ versus $t$ were fitted in Figs. 6 and 7. The adsorption kinetic parameters of pseudo-first-order and pseudo-second-order kinetic models were calculated from the intercept and slope of the linear relation and shown in Table 1. It was indicated that U(VI) adsorption on HCSs and HCSs-BDBPD follows the pseudo-second-order kinetic model owning to the good fit (both $R^2 > 0.99$) and approximately experimental and calculated $q_e$ with the model. The results demonstrated that U(VI) adsorption on HCSs and HCSs-BDBPD were controlled by chemical adsorption. The chemisorptions involves valence forces through sharing or exchanging electrons between HCSs (HCSs-BDBPD) and U(VI). Furthermore, chemical adsorption capacity is proportional to the number of actives sites occupied on the adsorbent surface [38].

## The effect of initial uranium concentration

The effect of initial U(VI) concentration on adsorption behavior was systematically investigated over a concentration range from 0 to 130 mg/L at pH 6.0 and 298.15 K within 90 min. The results showed in Fig. 8. Obviously, increasing the U(VI) concentrations lead an increase in the amount of U(VI) adsorbed on HCSs and HCSs-BDBPD within 70 and 90 mg/L, respectively. And then the capacity gradually reached equilibrium state and reached maximum capacity approximately 63 and 321 mg/g respectively. The comparision of capacity of U(VI) on various hydrothermal carbon materials were listed in Table 2 and showed that
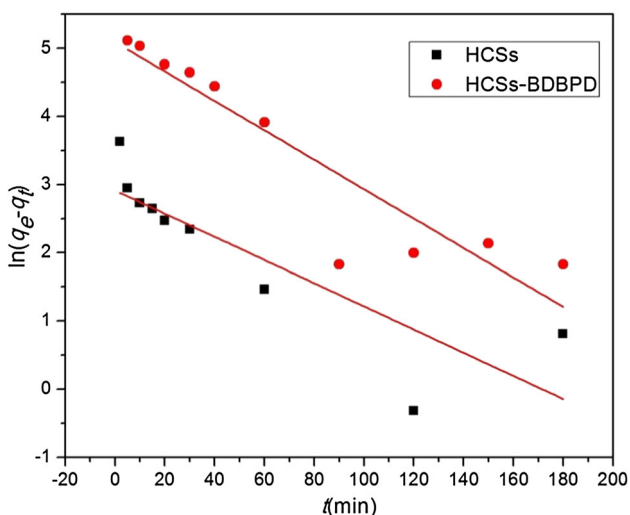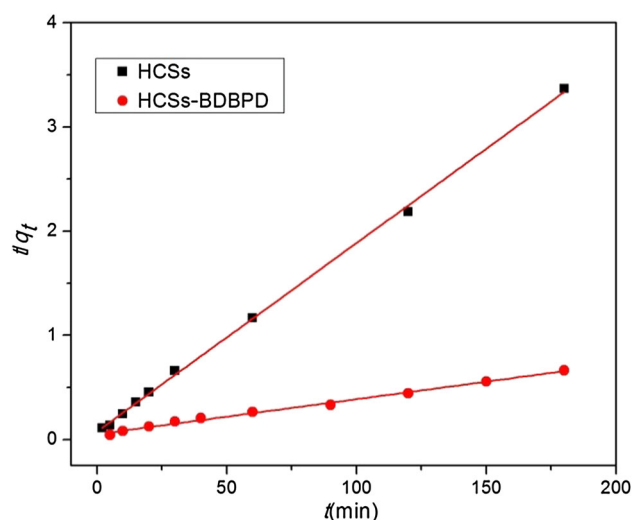


**Fig. 7** Pseudo-second-order adsorption kinetic of U(VI) over HCSs and HCSs-BDBPD

HCSs-BDBPD possess the much higher adsorption capacity than other hydrothermal carbon materials.

In order to describe U(VI) adsorption onto the adsorbent surface, two well-known adsorption models namely Langmuir and Freundlich were applied.

The linearized form of Langmuir and Freundlich equation is given as follows (4) and (5), respectively. The Fig. 9 is Langmuir fitting curve and Fig. 10 is Freundlich fitting figure.

$$\frac{C_e}{q_e} = \frac{1}{q_m K_L} + \frac{C_e}{q_m} \tag{4}$$

$$\ln q_e = \ln K_F + \frac{1}{n} \ln C_e \tag{5}$$

where $C_e$ (mg/L) and $q_e$ (mg/g) are the solution equilibrium concentration and the amount of solution adsorbed per unit mass of the adsorbent, $q_m$ is the maximum adsorption capacity (mg/g), $K_L$ is the Langmuir constant. $K_F$ and $n$ are the Freundlich constants.

The parameters such as $q_m$, $K_L$, $n$, $K_F$ and correlation coefficients ($R^2$), calculated from the slopes and intercepts of the plots of $C_e/q_e$ versus $C_e$ and $\ln q_e$ versus $\ln C_e$ are listed in Table 3. Comparison results of $R^2$ value shown in Table 3 demonstrates that the Langmuir isotherm fits the experimental data of HCSs and HCSs-BDBPD surfaces better than the Freundlich isotherm. The validity of Langmuir isotherm suggests that U(VI) adsorption is a monolayer process and adsorption of all U(VI) species requires equal activation energy [39]. The saturation capacity $q_m$ of HCSs and HCSs-BDBPD were 80 and 357 mg/g, respectively, proving HCSs-BDBPD had better adsorption capacity than HCSs.



**Fig. 6** Pseudo-first-order adsorption kinetic of U(VI) over HCSs and HCSs-BDBPD

**Table 1** Kinetic parameters of U (VI) adsorption onto HCSs and HCSs-BDBPD

| Sorbents | $q_{e,exp}$ (mg g$^{-1}$) | Pseudo-first-order adsorption | | | Pseudo-second-order adsorption | | |
|---|---|---|---|---|---|---|---|
| | | $q_{e,cal}$ (mg g$^{-1}$) | $k_1$ (min$^{-1}$) | $R^2$ | $q_{e,cal}$ (mg g$^{-1}$) | $k_2$ (g mg$^{-1}$ min$^{-1}$) | $R^2$ |
| HCSs | 54.97 | 18.44 | $1.7 \times 10^{-2}$ | 0.70 | 55.24 | $4.2 \times 10^{-3}$ | 0.995 |
| HCSs-BDBPD | 270.79 | 187.24 | $2.5 \times 10^{-2}$ | 0.87 | 294.12 | $2.2 \times 10^{-4}$ | 0.996 |
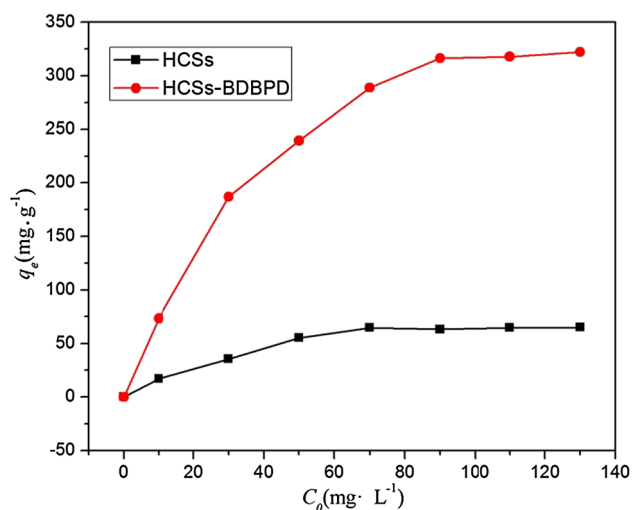


**Fig. 8** The effect of initial concentration of U(VI) on HCSs and HCSs-BDBPD adsorption properties

### The effect of temperature

Temperature is also a very important parameter on adsorption property of sorbent. The results indicated that the adsorption capacity of both HCSs and HCSs-BDBPD increased as absolute temperature increased from 298.15 to 318.15 K. In order to further research the adsorption principle, the thermodynamic parameters such as standard enthalpy change ($\Delta H$), standard entropy change ($\Delta S$) and standard Gibbs free energy change ($\Delta G$) for U(VI)

adsorption on HCSs and HCSs-BDBPD can be calculated from the temperature dependent adsorption isotherms.

The $\Delta H$ and $\Delta S$ can be calculated as Eq. (6):

$$\ln K_d = \frac{\Delta S}{R} - \frac{\Delta H}{RT} \tag{6}$$

where $K_d$ is the distribution coefficient (mL/g), $T$ and $R$ are the absolute temperature (K) and the gas constant (8.314 J mol$^{-1}$ K$^{-1}$), respectively. The values of $\Delta H$ and $\Delta S$ were derived from the slop and intercept of the plots of $\ln K_d$ versus $T^{-1}$ (Fig. 11).

Therefore, the values of $\Delta G$ can be obtained as Eq. (7):

$$\Delta G = \Delta H - T\Delta S = -TR \ln K_d \tag{7}$$

The values of $\Delta H$, $\Delta S$ and $\Delta G$ are tabulated in Table 4. The positive values of $\Delta S$ (101.89 and 121.74 J·K$^{-1}$·mol$^{-1}$) suggest that the adsorption process is irreversible. The positive values of $\Delta H$ and negative values of $\Delta G$ confirmed that the sorption process was endothermic spontaneous under all conditions tested, and the more negative value of $\Delta G$ at higher temperature indicated that the higher temperature was beneficial to the U(VI) sorption on HCSs and HCSs-BDBPD.

### Selectivity

For exploring the competitive adsorption behavior of U(VI) and other co-existing metal ions onto the surface of HCSs and HCSs-BDBPD. The batch sorption experiment in

**Table 2** Comparison of sorption capacity of U(VI) on various hydrothermal carbon materials

| Sorbents | Experimental conditions | Capacity (mg g$^{-1}$) | Reference |
|---|---|---|---|
| HCC produced with chitosan | pH = 7.92, $T$ = 338.15 K | 264.55 | [14] |
| CSs synthesized with glucose | pH = 6.0, $T$ = 298 K | 68.71 | [27] |
| HTC-PO$_4$ synthesized in the presence of phosphoric acid | pH = 5.0, $T$ = 298.15 K | 285.7 | [18] |
| HTC produced with pine needles | pH = 6.0, $T$ = 298 K | 62.7 | [38] |
| HCSs through low-temperature heat treatment | pH = 7.0, $T$ = 298.15 K | 179.95 | [25] |
| Salicylideneimine-functionalized HTC (HTC-sal) | pH = 4.3, $T$ = 288.15 K | 261 | [41] |
| Phenolic ligand-functionalized HTC (HTC-btg) | pH = 4.5, $T$ = 298.15 K | 307.3 | [40] |
| Bis-3,4-dihydroxybenzy)p-phenylen diamine-grafted hydrothermal carbon spheres (HCS-BDBPD) | pH = 6.0, $T$ = 298.15 | 321 | This work |
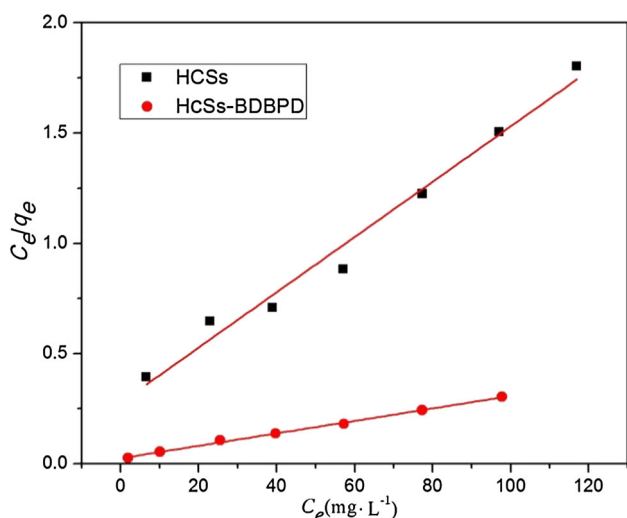
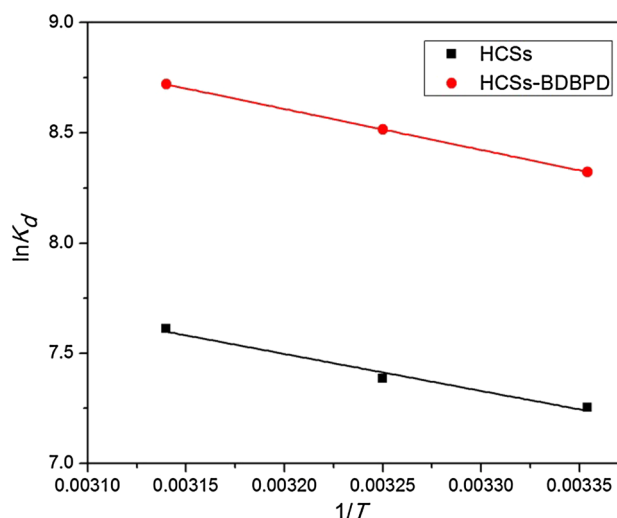Fig. 9 Langmuir isotherms adsorption of U(VI) on HCSs and HCSs-BDBPD



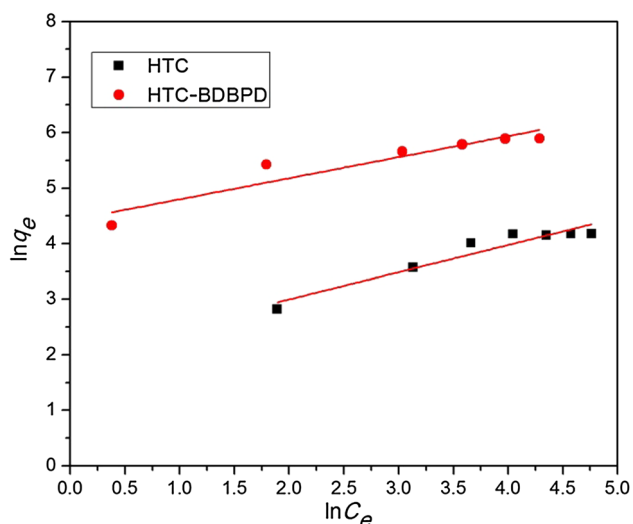Fig. 11 The variation of $\ln K_d$ versus $1/T$ for adsorption of U(VI) on HCSs and HCSs–BDBPD



Fig. 10 Freundlich isotherms adsorption of U(VI) on HCSs and HCSs-BDBPD

**Table 3** Parameters of Langmuir and Freundlich isotherm for adsorption of U(VI) onto HCSs

| Sorbent | Langmuir | | | Freundlich | | |
|---|---|---|---|---|---|---|
| | $K_L$ | $q_m$ (mg g$^{-1}$) | $R^2$ | $K_F$ | $n$ | $R^2$ |
| HCSs | 0.05 | 80.00 | 0.98 | 7.55 | 2.05 | 0.92 |
| HCSs-BDBPD | 0.11 | 357.14 | 0.99 | 66.00 | 2.65 | 0.95 |

simulated nuclear industry effluent containing several competing ions was carried out to investigate the selectivity of the sorbent. The results were represented in

Fig. 12. It was very clearly showed that the sorption amount of uranium onto HCSs and HCSs-BDBPD are much better than that of other co-existing cations. Comparing with HCSs, the sorption amount of HCSs-BDBPD towards U(VI) rises from 15.19 to 36.52 mg/g (pH = 6.0, $T = 298.15$ K, $C_0 = 10$ mg/L for uranium and other cations, $m = 40$ g for sorbents). It was confirmed that HCSs-BDBPD possesses better sorption capacity toward uranium than that of HCSs. Moreover, the sorption amount of co-existing ions onto the HCSs-BDBPD was greater than HCSs.

Simultaneously, the selectivity coefficient ($S$) and relative selectivity coefficient ($S_r$) were introduced to further evaluate the U(VI) selective sorption specialty of the sorbents. The $S$ and $S_r$ were calculated as following Eq. (8) and (9).

$$S = \frac{K_d^{UO_2^{2+}}}{K_d^{M^{n+}}} \tag{8}$$

$$S_r = \frac{S_{HCSs-BDBPD}}{S_{HCSs}} \tag{9}$$

where $K_d^{UO_2^{2+}}$ (ml/g) and $K_d^{M^{n+}}$ (mL/g) are distribution coefficients of uranyl ion and co-existing ions, respectively. The results are listed in Table 5. It was clear that the values of $K_d$ and $S$ of HCSs-BDBPD are much greater than that of HCSs. Furthermore, the value of Sr was over 10 for HCSs-BDBPD to Mg(II), Na(I) and Sr (II). These results indicated that the selective property of HCSs toward U(VI) was improved after grafting BDBPD groups on the surface of HCSs.

**Table 4** The thermodynamic parameters for adsorption of U(VI) onto HCSs and HCSs–BDBPD

| Sorbent | $\Delta H$ (kJ mol$^{-1}$) | $\Delta S$ (JK$^{-1}$ mol$^{-1}$) | $\Delta G$ (kJ mol$^{-1}$) | | |
|---|---|---|---|---|---|
| | | | 288.15 K | 298.15 K | 308.15 K |
| HCSs | 12.44 | 101.89 | −16.90 | −17.92 | −18.94 |
| HCSs-BDBPD | 15.67 | 121.74 | −20.62 | −21.84 | −23.05 |
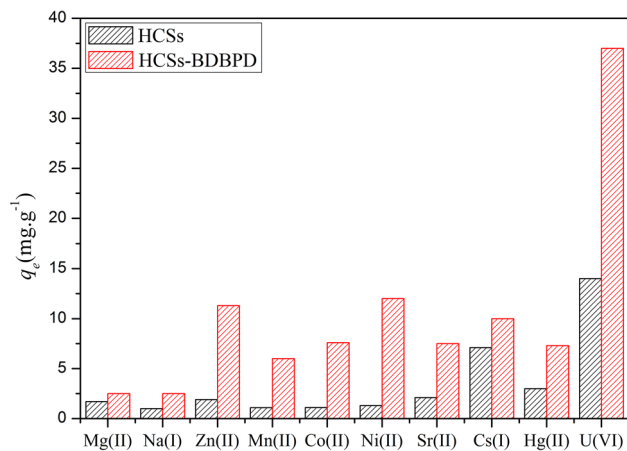


**Fig. 12** Competitive sorption capacities of HCSs and HCSs-BDBPD for U (VI) over competing ions in a simulated nuclear industrial effluent

**Table 5** Distribution coefficient and selectivity coefficients of HCSs and HCSs-BDBPD

| Ion | $K_d$ (mL g$^{-1}$) | | $S$ | | $S_r$ |
|---|---|---|---|---|---|
| | HCSs | HCSs-BDBPD | HCSs | HCSs-BDBPD | |
| U(VI) | 2552.63 | 140,211.95 | – | – | – |
| Mg(II) | 159.84 | 268.81 | 15.97 | 521.59 | 32.66 |
| Na(I) | 64.87 | 272.99 | 39.35 | 513.61 | 13.05 |
| Zn(II) | 164.24 | 1555.95 | 15.54 | 90.11 | 5.80 |
| Mn(II) | 78.81 | 647.42 | 32.39 | 216.57 | 6.69 |
| Co(II) | 85.78 | 999.38 | 29.76 | 140.30 | 4.71 |
| Ni(II) | 92.89 | 1824.75 | 27.48 | 76.84 | 2.80 |
| Sr(II) | 195.33 | 888.34 | 13.07 | 157.84 | 12.08 |
| Cs(I) | 775.35 | 1393.01 | 3.29 | 100.65 | 30.57 |
| Hg(II) | 280.04 | 876.63 | 9.12 | 159.94 | 17.55 |

## Possible adsorption mechanism

The possible interaction mechanism between U(VI) and HCSs-BDBPD under molecular level was shown in Fig. 13. U(VI) was coordinated with nitrogen-atoms and hydroxyl oxygen of BDBPD functional group [26]. Therefor, chelation is the main interaction mechanism between U(VI) and HCSs-BDBPD.
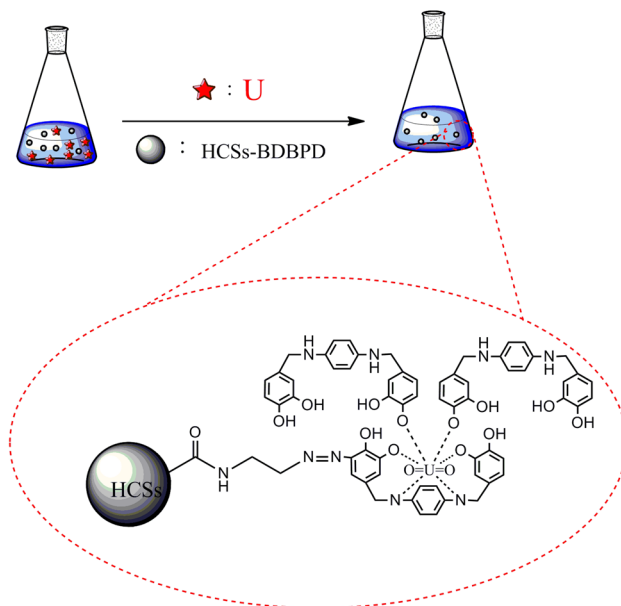


**Fig. 13** The possible interaction mechanism between U(VI) and HCSs-BDBPD

## Conclusion

In the present work, the adsorption property of HCSs-BDBPD synthesized successfully by hydrothermal method was investigated. The structure and textural property characterized by SEM and FT-IR showed that the BDBPD was successfully grafted to HCSs. The HCSs-BDBPD showed the maximum U(VI) adsorption capacity at initial pH of 6.0 and contact time of 90 min. The uranium sorption on HCSs and HCSs-BDBPD was well fitted to the Langmuir adsorption isotherm and pseudo-second-order kinetic model. The thermodynamic parameters distinctly revealed that the adsorption process was feasible, spontaneous and endothermic under tested condition. Moreover, the selectivity of the HCSs was improved after grafting BDBPD groups on HCSs. These results indicated that the synthesized HCSs-BDBPD might be a potential candidate for application in treatment and separation of uranium from the nuclear industrial effluents and other uranium contaminated aqueous media.

# References

1. Giri S, Singh G, Gupta SK, Jha VN, Tripathi RM (2010) An evaluation of metal contamination in surface and groundwater around a proposed uranium mining site, Jharkhand, India. Mine Water Environ 3:225–234

2. Singh SP, Hendry MJ (2012) Solid-phase distribution and leaching Behaviour of nickel and uranium in a uranium waste-rock piles. Water Air Soil Pollut 224(1):1–11

3. Biswas S, Pathak PN, Singh DK, Roy SB, Manchanda VK (2011) Mathematical modeling of solvent extraction of uranium from sulphate media employing 2-ethylhexyl phosphonic acid-mono-2-ethylhexyl ester (PC88A) and its mixture with trioctylphosphine oxide (TOPO) as extractants. J Radioanal Nucl Chem 2:557–564

4. Bermudez GMA, Moreno M, Invernizzi R (2010) Evaluating top soil trace element pollution in the vicinity of a cement plant and a former open-cast uranium mine in central Argentina. J Soils Sediments 7:1308–1323

5. Marshall TA, Morris K, Law GTW, Livens FR, Mosselmans JFW, Bots P, Shaw S (2014) Incorporation of uranium into hematite during crystallization from ferrihydrite. Environ Sci Technol 7:3724–3731

6. Gallegos TJ, Fuller CC, Webb SM, Betterton W (2013) Uranium(VI) interactions with mackinawite in the presence and absence of bicarbonate and oxygen. Environ Sci Technol 13:7357–7364

7. Ohnuki T, Ozaki T, Yoshida T, Sakamoto F, Kozal N, Wakal E, Francis AJ, Iefuji H (2005) Mechanisms of uranium mineralization by the yeast Saccharomyces cerevisiae. Geochim Cosmochim Acta 22:5307–5316

8. Alexandratos SD (2009) Ion-exchange resins: a retrospective from industrial and engineering Chemistry research. Ind Eng Chem Res 1:388–398

9. Zagorodnyaya AN, Abisheva ZS, Sharipova AS, Sadykanova SE, Bochevskaya YG, Atanova OV (2013) Sorption of rhenium and uranium by strong base anion exchange resin from solutions with different anion compositions. Hydrometallurgy 131–132(1):127–132

10. Li ZJ, Wang L, Yuan LY, Xiao CL, Mei L, Zheng LR, Zhang J, Yang JH, Zhao YL, Zhu ZT, Chai ZF, Shi WQ (2015) Efficient removal of uranium from aqueous solution by zero-valent iron nanoparticle and its graphene composite. J Hazard Mater 290:26–33

11. Pulhani VA, Dafauti S, Hegde AG (2011) Separation of uranium from iron in ground water samples using ion exchange resins. J Radioanal Nucl Chem 2:299–302

12. Nikoloski AN, Ang KL (2013) Review of the application of ion exchange resins for the recovery of platinum-group metals from hydrochloric acid solutions. Miner Process Extr Metall Rev 6:369–389

13. Yu XF, Liu YH, Zhou ZW, Xiong GX, Cao XH, Li M, Zhang ZB (2014) Adsorptive removal of U(VI) from aqueous solution by hydrothermal carbon spheres with phosphate group. J Radioanal Nucl Chem 3:1235–1244

14. Zhang WL, Zhang ZB, Cao XH, Ma RC, Liu YH (2014) Uranium adsorption studies on hydrothermal carbon produced by chitosan using statistical design method. J Radioanal Nucl Chem 301:197–205

15. Zou YD, Cao XH, Luo XP, Liu Y, Hua R, Liu YH, Zhang ZB (2015) Recycle of U(VI) from aqueous solution by situ phosphorylation mesoporous carbon. J Radioanal Nucl Chem 2:515–525

16. Nie WB, Zhang ZB, Cao XH, Liu YH, Liang P (2012) Sorption study of uranium from aqueous solution on ordered mesoporous carbon CMK-3. J Radioanal Nucl Chem 1:663–670

17. Tian G, Geng JX, Jin YD, Wang CL, Li SQ, Chen Z, Wang H (2011) Sorption of uranium(VI) using oxime-grafted ordered mesoporous carbon CMK-5. J Hazard Mater 1–3:442–450

18. Zhang ZB, Zhou ZW, Cao XH, Liu YH, Xiong GX, Liang P (2013) Removal of uranium(VI) from aqueous solutions by new phosphorus-containing carbon spheres synthesized via one-step hydrothermal carbonization of glucose in the presence of phosphoric acid. J Radioanal Nucl Chem 3:1479–1487

19. Yung MC, Ma J, Phinney MRBS, Bowman GR, Jiao Y (2014) Shotgun proteomic analysis unveils survival and detoxification strategies by Caulobacter crescentus during exposure to uranium, chromium, and cadmium. J Proteome Res 4:1833–1847

20. Kumar J, Mallampati R, Adin A, Valiyaveettil S (2014) Functionalized carbon spheres for extraction of nanoparticles and catalyst support in water. ACS Sustainable Chem Eng 12:2675–2682

21. Bhatta LKG, Subramanyam S, Chengala MD, Bhatta UM, Venkatesh K (2015) Enhancement in $CO_2$ adsorption on hydrotalcite-based material by novel carbon support combined with $K_2CO_3$ impregnation. Ind Eng Chem Res 54(43):10876–10884

22. Wang H, Ma LJ, Cao KC, Geng JX, Liu J, Song Q, Yang XD, Li SJ (2012) Selective solid-phase extraction of uranium by salicylideneimine-functionalized hydrothermal carbon. J Hazard Mater 229:321–330

23. Chen YQ, Guo JL (2014) Reversible oxidation of graphene through ultraviolet/ozone treatment and its nonthermal reduction through ultraviolet irradiation. J Phys Chem C 118(47):6407–6412

24. Titirici MM, Antonietti M (2010) Chemistry and materials options of sustainable carbon materials made by hydrothermal carbonization. Chem Soc Rev 1:103–116

25. Zhang ZB, Nie WB, Li Q, Xiong GX, Cao XH, Liu YH (2013) Removal of uranium(VI) from aqueous solutions by carboxyl-rich hydrothermal carbon spheres through low-temperature heat treatment in air. J Radioanal Nucl Chem 1:361–368

26. Bi C, Fang Y, Sun G, Chang J (1999) Synthesis and characterization of Th(IV) and U (VI) complexes with o-vanillin-p-phenylenediamine. J Radioanal Nucl Chem 246(1):221–223

27. Zhang ZB, Liu YH, Cao XH, Liang P (2012) Sorption study of uranium on carbon spheres hydrothermal synthesized with glucose from aqueous solution. J Radioanal Nucl Chem 3:1775–1782

28. Fanning PE, Vannice MA (1993) A drifts study of the formation of surface groups on carbon by oxidation. Carbon 31(93):721–730

29. Sun X, Li Y (2005) Ag@ C core/shell structured nanoparticles: controlled synthesis, characterization and assembly. Langmuir 21(13):6019–6024

30. Chen Z, Ma L, Li S, Geng S, Song Q, Liu J (2011) Simple approach to carboxyl-rich materials through low-temperature heat treatment of hydrothermal carbon in air. Appl Surf Sci 257(20):8686–8691

31. Zhang CX, Ren ZY, Yin ZG, Qian HY, Ma DZ (2007) Amide II and amide III bands in polyurethane model soft and hard segments. Polym Bull 1:97–101

32. Mamatov GZ, Yagu MR (1968) Integral intensities of the infrared bands due to the stretching. J Appl Spectrosc 8(5):825–829

33. O'Bannon E, Williams Q (2015) Vibrational spectra of four polycyclic aromatic hydrocarbons under high pressure: implications for stabilities of PAHs during accretion. Phys Chem Miner 66(4):872–875

34. Kross RD, Fassel VA, Margosiies M (1956) The infrared spectra of aromatic compounds. 11. evidence concerning the interaction of r-electrons and a-bond orbitals in C-H out-of-plane bending vibrations. J Am Chem Soc 78(7):1332–1335

35. Gu ZX, Wang Y, Tang J, Yang JJ, Liao JL, Yang YY, Liu N (2014) The removal of uranium(VI) from aqueous solution by graphene oxide–carbon nanotubes hybrid aerogels. J Radioanal Nucl Chem 303(3):1835–1842

36. Cheng HG, Zeng KF, Yu JT (2013) Adsorption of uranium from aqueous solution by graphene oxide nanosheets supported on sepiolite. J Radioanal Nucl Chem 1:599–603

37. Liu SJ, Ma JG, Zhang WQ, Luo F, Luo MB, Li FQ, Wu LP (2015) Three-dimensional graphene oxide/phytic acid composite for uranium(VI) sorption. J Radioanal Nucl Chem 2:507–514

38. Zhang ZB, Cao XH, Liang P, Liu YH (2012) Adsorption of uranium from aqueous solution using biochar produced by hydrothermal carbonization. J Radioanal Nucl Chem 2:1201–1208

39. Tan LC, Liu Q, Song DL, Jing XY, Liu JY, Li RM, Hu SX, Liu LH, Liu J (2015) Uranium extraction using a magnetic $CoFe_2O_4$–graphene nanocomposite: kinetics and thermodynamics studies. New J Chem 4:2832–2838

40. Li B, Ma L, Tian Y (2014) A catechol-like phenolic ligand-functionalized hydrothermal carbon: one-pot synthesis, characterization and sorption behavior toward uranium. J Hazard Mater 271:41–49

41. Wang H, Ma L, Cao K, Geng J, Liu J, Song Q, Li S (2012) Selective solid-phase extraction of uranium by salicylideneimine-functionalized hydrothermal carbon. J Hazard Mater 229:321–330